Surface changes on comet 67P/Churyumov-Gerasimenko suggest a more active past

Authors: M. Ramy El-Maarry[1, 2*], O. Groussin[3], N. Thomas[1], M. Pajola[4], A.-T. Auger[3], B. Davidsson[5], X. Hu[6], S. F. Hviid[7], J. Knollenberg[7], C. Güttler[6], C. Tubiana[6], S. Fornasier[8], C. Feller[8], P. Hasselmann[8], J.-B. Vincent[7], H. Sierks[6], C. Barbieri[9], P. Lamy[10], R. Rodrigo[11, 12], D. Koschny[13], H. U. Keller[7, 14], H. Rickman[15, 16], M. F. A'Hearn[17], M. A. Barucci[8], J.-L. Bertaux[18], I. Bertini[9], S. Besse[13], D. Bodewits[17], G. Cremonese[19], V. Da Deppo[20], S. Debei[21], M. De Cecco[22], J. Deller[6], J. D. P. Deshapriya[8], M. Fulle[23], P. J. Gutierrez[24], M. Hofmann[6], W.-H. Ip[25], L. Jorda[3], G. Kovacs[6], J.-R. Kramm[6], E. Kührt[7], M. Küppers[13], L. M. Lara[24], M. Lazzarin[9], Z.-Yi Lin[25], J. J. Lopez Moreno[24], S. Marchi[26], F. Marzari[9], S. Mottola[7], G. Naletto[27, 28, 20], N. Oklay[7], A. Pommerol[1], F. Preusker[7], F. Scholten[7], X. Shi[6]

Affiliations:

[1]Physikalisches Institut, Universität Bern, Sidlerstrasse 5, 3012 Berne, Switzerland.

[2]Laboratory for Atmospheric and Space Physics, University of Colorado, 3665 Discovery Drive, CO 80301, USA.

[3]Aix Marseille Université, CNRS, LAM (Laboratoire d'Astrophysique de Marseille), UMR 7326, 13388 Marseille, France.

[4]NASA Ames Research Center, Moffett Field, CA 94035, USA.

[5]Jet Propulsion Laboratory, 4800 Oak Grove Drive, Pasadena, CA 91109, USA.

[6]Max-Planck-Institut für Sonnensystemforschung, Justus-von-Liebig-Weg 3, 37077 Göttingen, Germany.

[7]Deutsches Zentrum für Luft- und Raumfahrt (DLR), Institut für Planetenforschung, Rutherfordstraße 2, 12489 Berlin, Germany.

[8]LESIA, Observatoire de Paris, PSL Research University, CNRS, Univ. Paris Diderot, Sorbonne Paris Cité, UPMC Univ. Paris 06, Sorbonne Universités, 5 Place J. Janssen, Meudon Principal Cedex 92195, France.

[9]Department of Physics and Astronomy, University of Padova, Vicolo dell'Osservatorio 3, 35122 Padova, Italy.

[10] Laboratoire d'Astrophysique de Marseille, UMR 7326 CNRS & Université Aix-Marseille, 13388 Marseille Cedex 13, France.

[11]Centro de Astrobiología, Instituto Nacional de Técnica Aeroespacial, 28850 Torrejón de Ardoz, Madrid, Spain.

[12]International Space Science Institute, Hallerstraße 6, 3012 Berne, Switzerland.

[13]Operations Department, European Space Astronomy Centre/ESA, P.O. Box 78, 28691 Villanueva de la Cañada, Madrid, Spain.

[14]Institut für Geophysik und extraterrestrische Physik (IGEP), Technische Universität Braunschweig, Mendelssohnstr. 3, 38106 Braunschweig, Germany.

[15]Department of Physics and Astronomy, Uppsala University, Box 516, 75120 Uppsala, Sweden.

[16]Polish Academy of Sciences (PAS), Space Research Center, Bartycka 18A, 00716 Warsaw, Poland.

[17]Department of Astronomy, University of Maryland, College Park, MD 20742-2421, USA.

[18] Laboratoire Atmosphères, Milieux, Observations Spatiales (LATMOS), Centre national de la recherche scientifique/ Université de Versailles Saint-Quentin-en-Yvelines/Institut Pierre Simon Laplace, 11 Boulevard d'Alembert, 78280 Guyancourt, France.

[19] Istituto Nazionale di Astrofisica (INAF), Osservatorio Astronomico di Padova, Vicolo dell'Osservatorio 5, 35122 Padova, Italy.

[20]Consiglio Nazionale delle Ricerche (CNR)-Istituto Di Fotonica E Nanotecnologie (IFN), Unita' Organizzativa di supporto (UOS), Padova Luxor, Via Trasea, 7, 35131 Padova, Italy.

[21]Department of Industrial Engineering, University of Padova, Via Venezia, 1, 35131 Padova, Italy.

[22]University of Trento, via Sommarive, 9, 38123 Trento, Italy.

[23]INAF, Osservatorio Astronomico di Trieste, Via Tiepolo 11, 34014 Trieste, Italy.

[24]Instituto de Astrofisica de Andalucía (CSIC), c/ Glorieta de la Astronomía s/n, 18008 Granada, Spain.

[25]Graduate Institute of Astronomy, National Central University, 300 Chung-Da Rd, Chung-Li 32054, Taiwan.

[26]Solar System Exploration Research, Virtual Institute, Southwest Research Institute, 1050 Walnut St., Suite 300, Boulder, CO 80302, USA.

[27]Department of Information Engineering, University of Padova, Via Gradenigo 6/B, 35131 Padova, Italy.

[28]Centro di Ateneo di Studi ed Attivitá Spaziali "Giuseppe Colombo" (CISAS), University of Padova, Via Venezia 15, 35131 Padova, Italy.

*Correspondence to: (mohamed.elmaarry@lasp.colorado.edu).

Abstract: The Rosetta spacecraft spent nearly two years orbiting Comet 67P/Churyumov-Gerasimenko, most of it at distances that allow surface characterization and monitoring at sub-meter scales. From December 2014 to June 2016, numerous localized changes were observed, which we attribute to cometary-specific weathering, erosion, and transient events driven by exposure to sunlight and other processes. While the localized changes suggest compositional or physical heterogeneity, their scale has not resulted in substantial alterations to the comet's landscape. This suggests that most of the major landforms were created early in the comet's current orbital configuration. They may even date from earlier if the comet had a larger volatile inventory, particularly of CO/CO_2 ices, or contained amorphous ice, which could have triggered activity at larger distances from the Sun.

One Sentence Summary: Comets' surfaces change on seasonal scales, displaying evidence for weathering, intensive localized erosion, and unique short-scale morphological changes.

Main Text:

The ~2 year-long Rosetta mission (Aug. 2014–Sep. 2016) at Comet 67P/Churyumov-Gerasimenko (hereafter referred to as 67P) allowed mapping the entire surface of the nucleus at sub-meter resolution, and closely monitoring it during its journey through the inner solar system. The initial characterization following arrival in Aug 2014 (*1*) showed 67P's surface to be diverse in its morphology, comprising different surface textures, which included rough consolidated terrains, smooth plains, unconsolidated mantles, and ubiquitous boulders (e.g., *2–5*). Following perihelion (on Aug 13, 2015), we carried out a comparative analysis of many regions of the comet's northern hemisphere and equatorial regions to look for morphological or physical changes since arrival (*6*). Here we present the most striking events observed using the Optical, Spectroscopic, and Infrared Remote Imaging System (OSIRIS, *7*).

Erosion (supplementary online text) on the surface of the comet appears to begin as in-situ weathering of consolidated surfaces, which acts to weaken these materials causing their fragmentation. This effect is evident in two locations where cliff collapses have taken place in the Seth (Fig. 1A,) and Ash (Fig. S2) regions (see Fig. S1 for region definitions). The collapsing material detached at the locations of pre-existing fractures, which were tens of meters long. Fractures play a major role in driving cliff failures on Earth (e.g. *9*). On 67P, the failures were probably initiated by insolation weathering as a fracturing process (10), and triggered by associated or nearby activity (*11*).

In the neck region, a large pre-existing >500 m-long fracture running through the northern neck extended by at least another 30 m (Figs. 1B, S3), along with possible development of new fractures parallel to it. The morphology and setting of these fractures is consistent with tensile fractures (*10, 12*), particularly the lack of additional splitting at the fracture tips (*12*). The earliest possible extension of the fracture was detected in Dec. 2014 images but most of the changes are evident in post-perihelion images (Fig. S3). 67P's spin rate increased steadily from May 2015 to a maximum near perihelion (*13, 14*) as a result of activity-induced torques (*13*). Recent finite-element models (*12*) suggest that increases in the spin rate could lead to development of tensile stresses in the neck region, which would lead to extension of pre-existing fractures and development of new ones, consistent with our observations. However, the presence of other linear features with differing orientations (Fig. 1B) suggests possible evolution of the stress regime with time.

In the southern/near-equatorial Khonsu region a 20×30×40 m-wide boulder moved a distance of ~140 m (Fig. 1C) during the period around perihelion (Fig. S4). Its volume of ~24,000 m^3 corresponds to a mass of 12.8 x 10^6 kg assuming bulk density of 533 kg/m^3 (*15*), which would be comparable to lifting a ~250 kg boulder on Earth. Images taken shortly before and after perihelion (Fig. S5) show multiple outburst events (intensive and localized jet activity) close to the boulder's position, which could be responsible for the movement of the boulder. Viable processes are erosion of the sloped surface on which the boulder resided, thus leading to its rolling downslope, or direct uplift if the outburst was strong enough, i.e. having a flux exceeding 25 kg s^{-1} (supplementary online text).

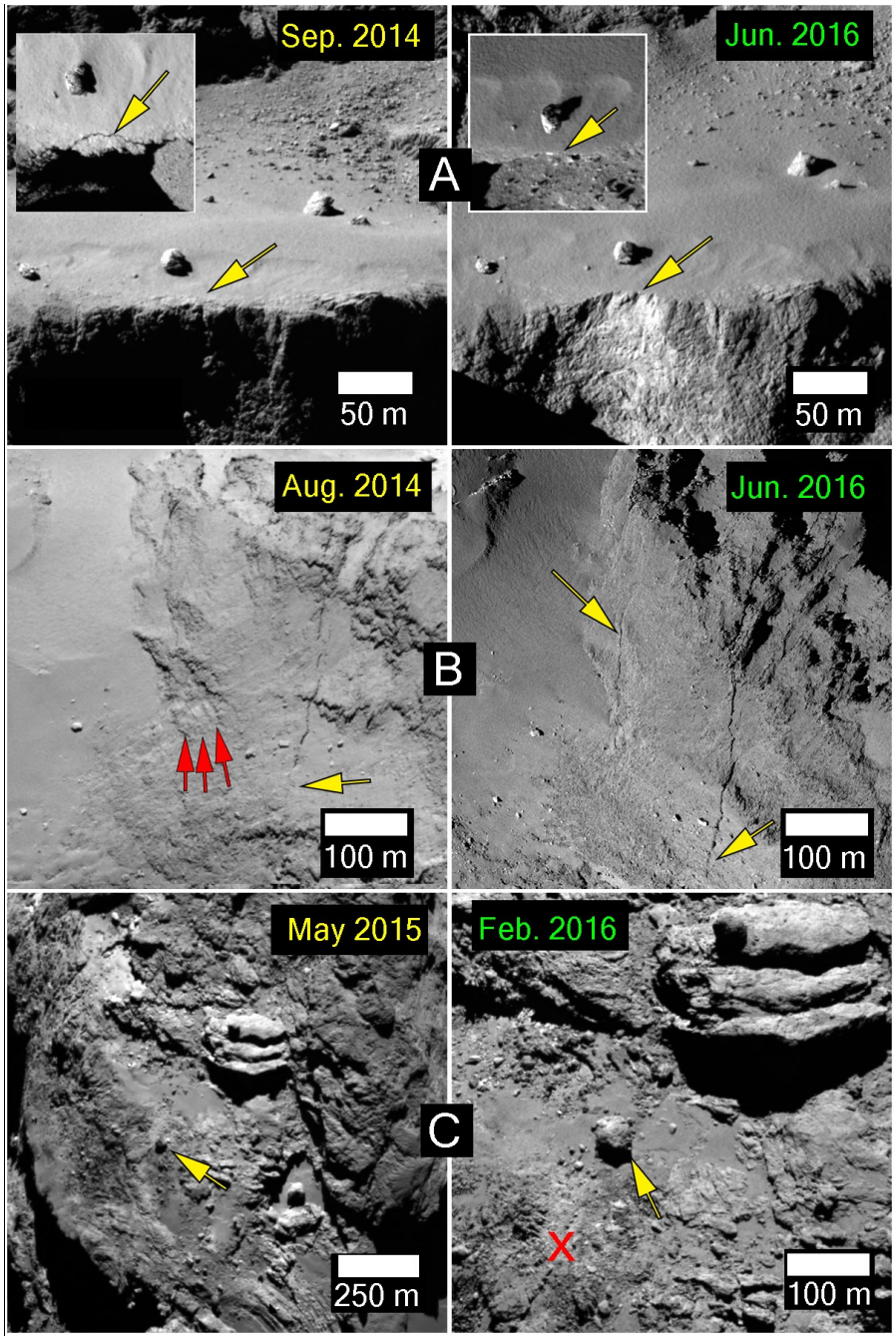

Fig. 1. Weathering-related changes on 67P. (A) Cliff collapse on the large lobe in a location named Aswan in the Seth region (*8*). The detached segment was ~12 m-wide and the fracture was ~50 m-long (*8*). (B) Extension of a pre-existing fracture in the neck region and the development of a new one parallel to it. Multiple lineaments are present with variable orientations (red arrows). (C) Movement of ~30 m-wide boulder for a distance of ~140 m in the Khonsu region (the letter x marks the original position in the right panel). In all panels, the yellow arrows point to the features of interest. Throughout the paper, the dates shown are the approximate acquisition date of the images. Their color indicates whether the image was acquired before (yellow) or after (green) perihelion. Additional details are in Table S1.

In addition to in-situ weathering, we have observed probable indicators of erosional transport of unconsolidated materials on the surface of 67P, resulting in the exhumation of previously covered surfaces. For example, the Imhotep region shows a diverse surface characterized by smooth terrains and unusual circular structures (*4*). One particular location in this region has been substantially exhumed to reveal previously covered circular features and boulders (Fig. 2). Using an image acquired at a distance of ~6 km from the surface (corresponding to a resolution of 0.11 m/pixel, Fig. 2C), we calculated the height of the exhumed section of a boulder to be $3.9^{+0.1}_{-0.2}$ m. The quoted uncertainty is the standard deviation corresponding to the inherent uncertainties in the Spacecraft and Planet Kernels (SPK). We discarded the highest point of the boulder from our measurements, as it was originally exposed (Fig. 2C). This estimate indicates that the extent of vertical erosion at this particular location exceeded 3 m.

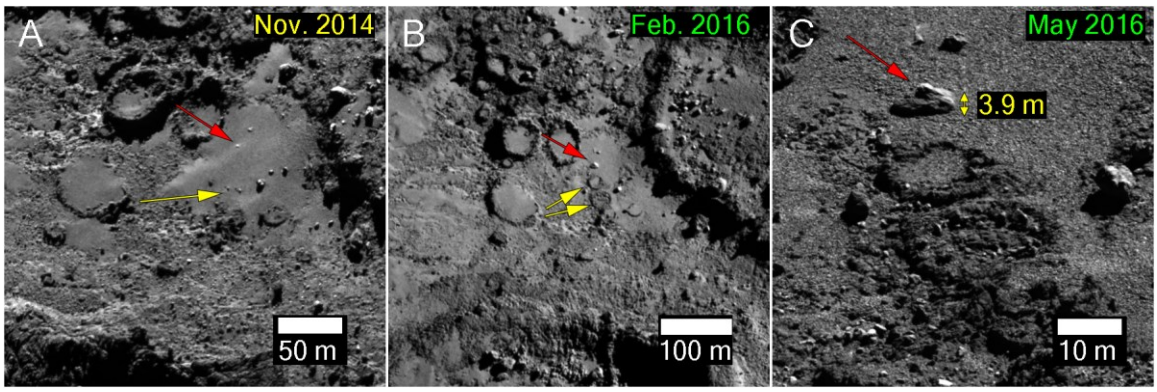

Fig. 2. Evidence of erosion in the Imhotep region. In all panels the direction of sunlight is from the upper right corner. (A) In Nov. 2014 a number of circular features are visible and a blanket of smooth materials almost completely covers a boulder (red arrow). The yellow arrow marks the location of two circular features exposed in later figures. (B) Two new circular features appear in this image taken in Feb. 2016. During this time, the boulder has been exhumed as well. (C) A higher-resolution image of the newly exposed features.

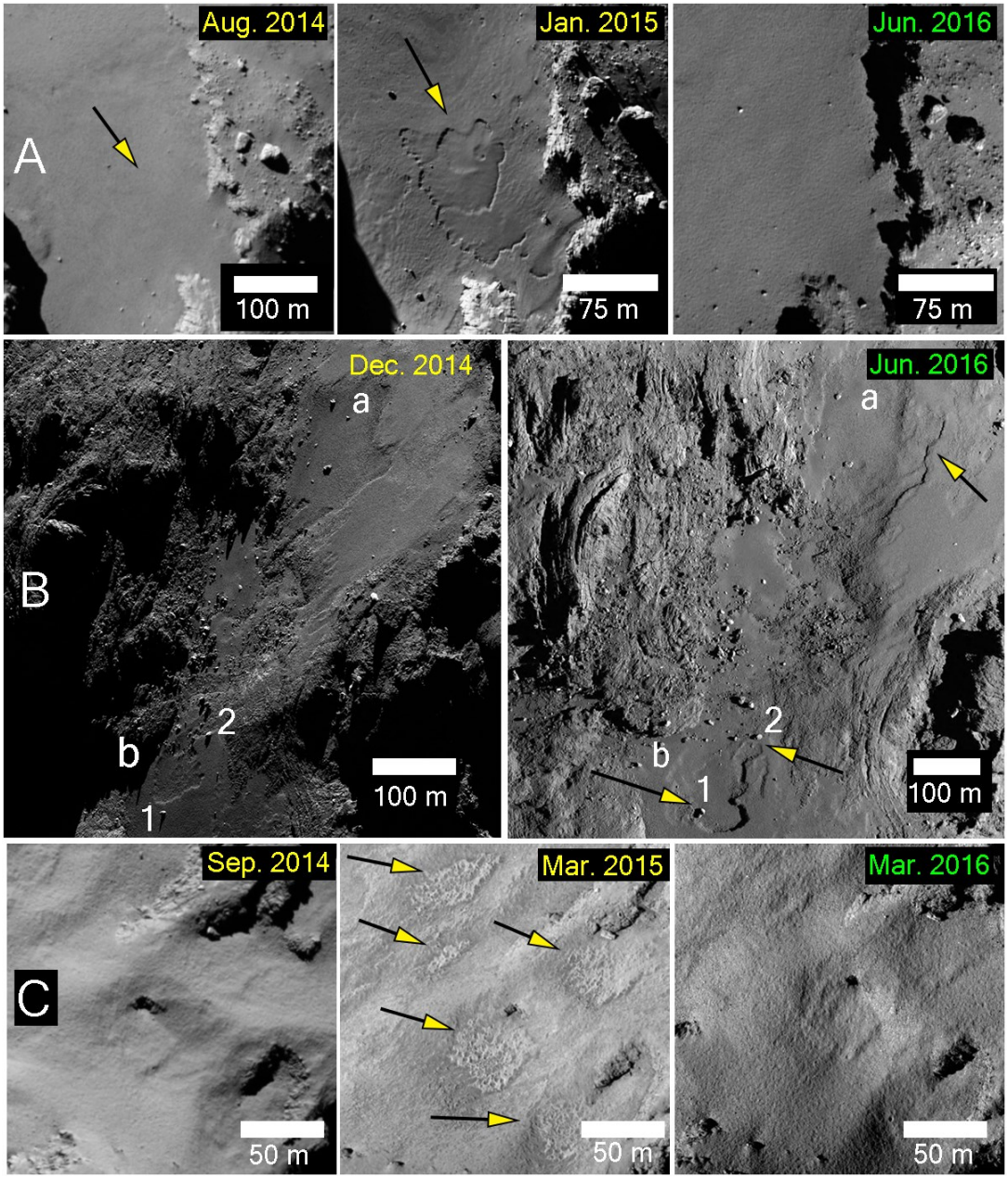

Fig. 3. Transient surface changes on 67P. (A) Part of the Hapi region (the northern neck) that appeared smooth and featureless in Aug. 2014, then displayed pit-and-scarp patterns early in 2015, which had disappeared by the time the area was re-imaged after perihelion. The middle and far right images were down-sampled to closely match the resolution of the left panel. (B) Distinctive morphological changes characterized by scarp retreat observed in the Anubis region, particularly in the areas marked a, and b (see Fig S6). Area b shows a retreat of the scarp in post perihelion bypassing boulder 1 and reaching another boulder 2 on the opposite side. (C) An area in the Ma'at region on the small lobe shows a smooth surface that underwent transient changes as the comet approached perihelion, creating honeycomb-like structures.

Another set of observations shows morphological changes that affect directly the unconsolidated materials. These changes are mainly transient since they fade away gradually with time as the

surface almost reverts to its original appearance. In smooth terrains such as Hapi (Fig. 3A), Anubis (Fig 3B), and Imhotep (*16*, Fig. S6), the changes are marked by the appearance and/or receding of shallow scarps (~1–5 m-deep from shadow measurements, supplementary online text) forming quasi-circular or pitted patterns. Some enlarge with time, and later stop their evolution (e.g., Anubis) or fade away (e.g., Hapi). During their evolution, many scarps display brightening (e.g., Fig. S7), indicative of exposed water ice using spectrophotometric analysis (*17,* supplementary online text, Fig. S8). A near-continuous time series of images around perihelion for the Anubis region indicates an average rate of scarp retreat of ~5.4 m/day at feature a (Fig. 3B and S9) close to perihelion, which is consistent with a similar range of values (4.3–7.6 m/day) observed at Imhotep (*16*). In total, features a and b displayed scarp retreats of ~35 m and ~50 m, respectively (supplementary online text). These values are markedly higher than similar changes at comet 9P/Tempel 1 (~25 m/orbit) [*18*], which could be attributed to a smaller perihelion distance for 67P (1.24 vs 1.5 astronomical units [au]).

Early in the mission, aeolian-like (forms commonly created by wind) ripples were seen in the Hapi region (2). The location became a nucleus for the development of similarly growing circular features by scarp retreat with associated brightening (Fig. S10). The circular features reached a diameter of ~100 m in less than 3 months, then faded away and created a new set of ripples. Recent models (*19*) predict that activity in the neck would generate high outgassing speeds (~500 m/s). These gases would then be funneled over the ripples area, perpendicular to their long axes due to the comet's irregular shape (*19*), which may explain the recurring nature of the ripples. In the Imhotep region, we observed similarly transient circular features (Fig. S11) on the smooth materials overlying the later-exhumed terrain (Fig. 2). Therefore, we can infer that the development of transient circular patterns, coupled with brightening, is an indicator of materials being actively eroded.

Finally, starting in Mar. 2015, numerous patches on the surface of dust-covered terrains (*2, 3*), particularly in the Ma'at region (Fig. 3C), underwent textural changes marked by increase in surface roughness to form honeycomb-like features (*20*). Similar to other seasonal changes, these features have faded substantially in post-perihelion images. The fading was probably due to resurfacing through deposition of new particles, likely those ejected from the southern hemisphere during intensive perihelion activity (*21*).

The substantial yet localized changes in the comet mainly occur around perihelion (Fig. 4A). Many of the events (e.g., boulder movement [Fig. 1C], erosion in Imhotep [Fig. 2], and transient changes [Fig. 3]) appear to be driven by insolation (exposure to sunlight) as they take place close to the corresponding sub-solar latitude (SSL, Fig. 4B). Exceptions include the fracture extension in the neck (Fig. 1B), which is related to the comet's spin rate; the pit-and-scarp patterns in the Hapi region (Fig 3A); and the cliff collapses (Figs. 1A, S1). The changes in Hapi can be attributed to the peculiar geometry of the northern neck leading to self-heating (infrared radiation emitted back from the comet) and earlier onset of activity (*21*). The collapsing cliffs are a special case because they receive more solar input when the vertical walls are illuminated compared to when the Sun is above them (i.e. at the SSL). Regardless, they occur around perihelion at distances < 2 au, similar to most observed changes. The deviation of the changes in Anubis from the SSL could be a result of the SSL's rapid shift during perihelion (Fig. 4B), and therefore an observational bias.

The changes in the smooth terrains occur around the same latitude (~10ºS) but appear as a chain of events rather than simultaneously. This could either indicate different thermo-physical surface

properties or geometrical factors,. For example, self-heating would trigger earlier activity in Hapi. Imhotep is relatively flat and is exposed to sunlight over a wider range of incidence angles than the smooth plains of Anubis, which are enclosed by higher elevated regions, therefore becoming active later. The highly localized nature of all the observed changes suggests compositional and/or physical heterogeneity on the comet's surface at the scale of the observed changes (i.e., tens of meters).

No major changes to the comet's landscape occurred that substantially altered its shape or major landforms, even in the southern hemisphere (where lower resolution, yet adequate, data is available from May 2015). Given that the comet has only spent <10 orbits in its current close configuration (since 1959 e.g., *22*), it is possible that earlier perihelion passages were more active than the one in 2015.That would provide the higher rates of change required to shape the comet. However, ground-based observations suggest similar levels of activity in previous orbits, though only as far back as 1982 (*23*). Alternatively, the comet's landscape may have evolved to its current form at a different phase of the comet's lifetime, possibly during its 1840 orbital configuration during which 67P had a perihelion distance of 2.74 au (*22*). This distance would still lead to active modification of the surface (Fig. 4) but would require more vigorous activity. That may have been possible if CO/CO_2 sublimation, rather than the more common H_2O sublimation, was involved (due to its activity at lower temperatures than H_2O and consequently activity at larger distances), and the comet had a higher inventory of it in the past. Exothermic crystallization of amorphous ices could have triggered higher rates of activity at earlier epochs, such as when comet 67P was in its Centaur phase (e.g., *24, 25*).

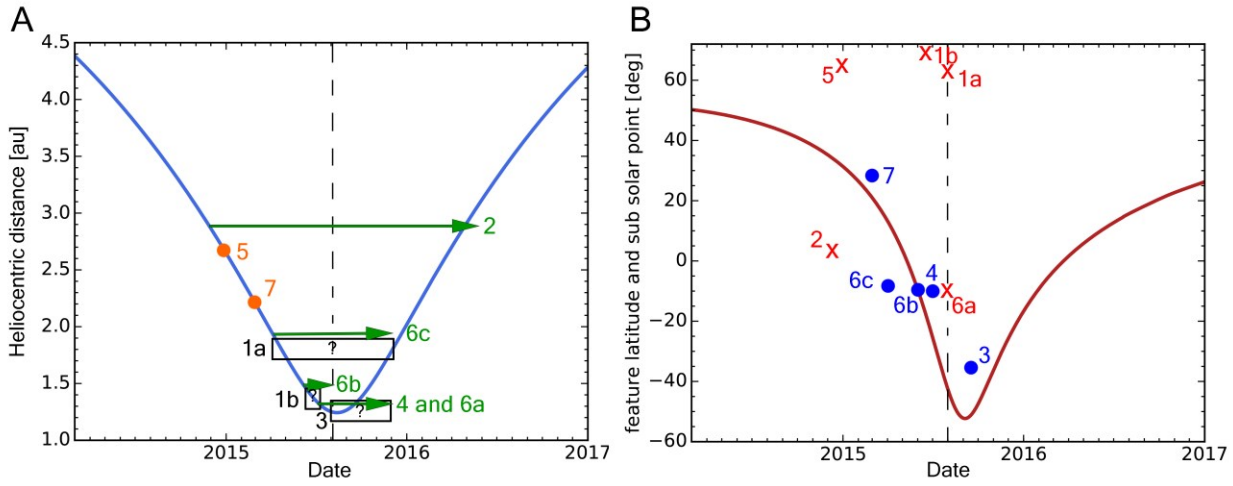

Fig. 4. Timing of the observed changes vs heliocentric distance (A) and sub solar latitude [SSL] (B). The solid lines show the evolution of the comet's heliocentric distance and the SSL, respectively. The dashed line indicates perihelion; TCP stands for transient circular patterns. Orange colors represent single events of confirmed time, green arrows represent continuous activity in a given period, and black boxes represent single events where the exact time is unknown but constrained to a given period. In panel B: blue dots signify events that appear to be insolation-driven, i.e. active within ±20º of the SSL. Red crosses represent events that appear to be driven by other processes. Additional information is in table S2.

References and Notes:

1. Sierks, H. et al. Science **347** (2015). DOI: 10.1126/science.aaa1044
2. Thomas, N. *et al*. Science **347,** (2015). DOI: 10.1126/science.aaa0440.
3. El-Maarry, M. R. *et al.* Astronomy & Astrophysics **583**, A-26 (2015).
4. Auger, A-T. *et al*. Astronomy & Astrophysics **583**, A-35 (2015).
5. Pajola, M. *et al*. Astronomy & Astrophysics **583**, A-37 (2015).
6. See Materials and Methods in the online supplementary material.
7. Keller, H. U. *et al.* Space Sci. Rev. **128**, 433–506 (2007).
8. Pajola, M. *et al*. Astronomy & Astrophysics **592,** A-69 (2016).
9. Duperret, A., Genter, A., Martinez, A., Mortimore, R. N. Geo. Soc., London, Eng. Geo. Spec. Pub. **20**, 33–55, (2004).
10. El-Maarry, M. R. *et al.* Geophys. Res. Lett. **42,** 5170–5178 (2015).
11. Vincent, J. -B. *et al.* Astronomy & Astrophysics **587,** A-14 (2016).
12. Hirabayashi, M. *et al.* Nature **534**, doi:10.1038/nature17670 (2016).
13. Keller, H. U., Mottola, S., Skorov, Y. & Jorda, L. Astronomy & Astrophysics **579,** L-5 (2015).
14. Jorda, L. *et al.* Icarus 277, 257–278 (2016).
15. Pätzold, M. *et al.* Nature **530**, 63–65 (2016).
16. Groussin, O. *et al.* Astronomy & Astrophysics **583**, A-36 (2015).
17. Fornasier, S. *et al*. Science, doi: 10.1126/science.aag2671.
18. Thomas, P. *et al*. Icarus **222**, 453–466 (2013).
19. Thomas, N. *et al*. Astronomy & Astrophysics **583**, A-17 (2015).
20. Shi, X. *et al*. Astronomy & Astrophysics **586,** A-7 (2016).
21. Keller, H. U. *et al.* Astronomy & Astrophysics **583,** A-34 (2015).
22. Belyaev, N., Kresak, L., Pittich. E. M., Catalogue of Short-Period Comets, Slovak Academy of Sciences, Astronomical Institute, Bratislava (1986).
23. Snodgrass, C. *et al*. Astronomy & Astrophysics. **588,** A-80 (2016).
24. Jewitt, D. Astronom. J. **137**, 4296–4312, (2009).
25. Prialnik, D and Bar-Nun, A. Astrophys. J., **313**, 893–905, (1987).
26. Tubiana, C. *et al.*, Astronomy & Astrophysics **583,** A-46 (2015).
27. Gombosi, T.I., Nagy, A. F., Cravens, T. E. Rev. Geophys. **24**, 667–700 (1986).
28. Fulle, M. Astronomy & Astrophysics **325**, 1237–1248 (1997).
29. Crifo, J. F. Astronomy & Astrophysics **223**, 365–368, (1989).
30. Bailey, A. B., Hiatt, J. Amer. Inst. Aeronautics & Astronautics J. **10**, 1436–1440, (1972).
31. Keller. H. U., Physics and Chemistry of Comets (ed. W.F. Huebner), Springer, 13–68, (1990).

Acknowledgments: The authors would like to thank 3 reviewers for their constructive suggestions that have improved this work. OSIRIS was built by a consortium of the Max-Planck-Institut für Sonnensystemforschung (MPS), in Göttingen, Germany; Centro Interdipartimentale di Studi e Attività Spaziali–University of Padova, Italy; the Laboratoire d'Astrophysique de Marseille, France; the Instituto de Astrofísica de Andalucia, Consejo Superior de Investigaciones Cientificas, Granada, Spain; the Research and Scientific Support Department of the European Space Agency (ESA), Noordwijk, Netherlands; the Instituto Nacional de Técnica Aeroespacial, Madrid, Spain; the Universidad Politećhnica de Madrid, Spain; the Department of Physics and

Astronomy of Uppsala University, Sweden; and the Institut für Datentechnik und Kommunikationsnetze der Technischen Universität Braunschweig, Germany. The support of the national funding agencies of Germany (Deutschen Zentrums für Luft- und Raumfahrt), France (Centre National d'Etudes Spatiales), Italy (Agenzia Spaziale Italiana), Spain (Ministerio de Educación, Cultura y Deporte), Sweden (Swedish National Space Board; grant no. 74/10:2), and the ESA Technical Directorate is gratefully acknowledged. H.R. was also supported bygrant no. 2011/01/B/ST9/05442 of the Polish National Science Center. W.-H.I acknowledges the Ministry of Science and Technology, Taiwan (grant no. NSC 101-2111-M-008-016). M.F.A. acknowledges NASA funding through Jet Propulsion Laboratory contract no. 1267923. The team from the University of Bern is supported through the Swiss National Science Foundation (grant no. 200020_165684) and through NCCR PlanetS. We thank the ESA teams at European Space Astronomy Centre, European Space Operations Centre, and European Space Research and Technology Centre for their work in support of the Rosetta mission. Rosetta/OSIRIS data are available through the ESA's Planetary Science Archive (PSA) http://www.cosmos.esa.int/web/psa/rosetta. Images used in this study that are not yet available at PSA can be downloaded from the MPS OSIRIS website, at https://planetgate.mps.mpg.de/WebFileShare/Released_Images/El-Maarry+Science/ .

Supplementary Materials:

Materials and Methods

Supplementary text S1–S5

Figures S1–S11

Tables S1–S2

References 26–31